ADVANCED OPTICAL MATERIALS
www.advopticalmat.de

Revealing Phonon Polaritons in Hexagonal Boron Nitride by Multipulse Peak Force Infrared Microscopy

*Le Wang, Martin Wagner, Haomin Wang, Siuling Pau-Sanchez, Jiahan Li, James H. Edgar, and Xiaoji G. Xu**

Probing of polaritons in 2D materials is facilitated by spectroscopic imaging with nanometer spatial resolution. The combination of atomic force microscopy and infrared laser sources provides access for in situ mappings of phonon polaritons. Here, it is demonstrated that the photothermal-based peak force infrared microscopy is capable of revealing phonon polaritons with high spatial resolution in isotopically pure hexagonal boron nitride microstructures without damaging the sample. To further improve the sensitivity, peak force infrared microscopy is enhanced with a scheme of multiple laser pulse excitation. The resulting method of multipulse peak force infrared microscopy can detect phonon polaritons with high sensitivity, which is particularly useful for probing polaritons in 2D materials with high damping characteristics.

Phonon polaritons (PhPs) are electromagnetic waves that originate from the coupling of hybridized lattice oscillations and nonpropagating evanescent field of photons. The wavelength of phonon polaritons is much shorter than that of free propagating infrared photons. As a result, they have been widely applied in the field of nanophotonics, from light harvesting, sensors, to confined light delivery. 2D materials, such as graphene, hexagonal boron nitride, and molybdenum disulfide, can support a variety of polaritons, including plasmon polaritons, phonon polaritons, and exciton polaritons, with wavelengths ranging from ultraviolet to far-infrared.[1,2]

However, the generation and spectroscopic detection of phonon polaritons by spectroscopy and microscopy are not straightforward. The generation of short-wavelength polaritons from long-wavelength photons of the same energy can be inefficient due to their momentum mismatch. Hence, to launch polaritons from far-field illumination, phase matching is required.[3] One way to achieve this is to spatially pattern 2D materials into periodical nanostructures with determined spatial frequencies that provide additional momenta to match the difference between free photons and polaritons. However, the small size of polaritonic nanostructures poses a challenge for conventional spectroscopy: Abbe's diffraction limit of microscopy prevents the nanoscale spatial resolution,[4] particularly in the phonon-active infrared range.

Combining optical excitation with atomic force microscopy (AFM) provides a way to satisfy phase matching and bypass the diffraction limit. The metallic tip of the AFM serves as a small optical antenna that locally confines the optical radiation, resulting in electromagnetic fields with a high spatial frequency that allows efficient coupling to polaritons.[5] The sharp tip is thus capable of launching polaritons even for planar 2D materials.[6] Moreover, the metallic AFM tip also serves as a local probe on the optical resonance of the sample, bypassing the optical diffraction limit.

AFM-based, scattering-type scanning near-field optical microscopy (s-SNOM) is a popular method for studying polaritons in 2D materials.[7] It detects the light scattered from a sharp metallic AFM tip. The charge distributions and motions due to optical excitation of the sample modify the polarizability of the metallic AFM tip, leading to resonance-dependent scattered signals.[8,9] s-SNOM can both excite polaritons with high momenta and detect them with high spatial resolution, thus it is suitable for studying polaritons in low dimensional materials.[9] Polaritons in BN,[2] $MoSe_2$,[10] MoO_3[11] were experimentally discovered and quantified by s-SNOM.

However, s-SNOM instrumentation is complex: it must deliver the laser radiation to the AFM tip and optically collect the near-field scattered light.[12] Furthermore, the amplitude of the s-SNOM signal does not correspond to the resonant profile of the sample. Consequently, it requires delicate interferometric optical detection schemes to measure the imaginary part (the phase of the near-field scattering signal), which is proportional to the optical absorption. Moreover, s-SNOM also requires expensive light sources if both imaging and spectroscopy capabilities are required: single frequency imaging uses a continuous-wave laser source, such as a quantum cascade laser;

Dr. L. Wang, H. Wang, Prof. X. G. Xu
Department of Chemistry
Lehigh University
6 E Packer Ave., Bethlehem, PA 18015, USA
E-mail: xgx214@lehigh.edu
Dr. M. Wagner
Bruker Nano Surfaces
112 Robin Hill Road, Santa Barbara, CA 93117, USA
S. Pau-Sanchez
Department of Physics
University of California
Santa Cruz, CA 95064, USA
Dr. J. Li, Prof. J. H. Edgar
Tim Taylor Department of Chemical Engineering
Kansas State University
Manhattan, KS 66506, USA
The ORCID identification number(s) for the author(s) of this article can be found under https://doi.org/10.1002/adom.201901084.

DOI: 10.1002/adom.201901084

spectroscopy typically requires broadband laser sources, such as femtosecond radiation from difference frequency generation. Currently, the high instrumentation cost limits the application of s-SNOM in material research.

Photothermal AFM-IR microscopy provides a simpler alternative to s-SNOM with equal resolution. This technique detects the photothermal expansion of the sample due to infrared excitation. The popular photothermal induced resonance (PTIR) technique provides a spatial resolution of 20 to 100 nm, depending on types of samples.[13,14] However, PTIR uses contact mode AFM, in which the AFM tip may scratch the sample surface during scanning, irreversibly changing the surface property.[15,16] The photo-induced force microscopy (PiFM) (and tapping mode AFM-IR, which shares a similar signal acquisition mechanism with PiFM) uses the tapping mode feedback and provides a good spatial resolution of 10 nm.[17,18] However, the signal generation mechanism of PiFM is under debate.[17,19]

Recently-developed peak force infrared (PFIR) microscopy is a new type of photothermal AFM-IR microscopy that overcomes the limitation of the contact mode PTIR microscopy.[20] PFIR microscopy operates in the peak force tapping mode[21] that can avoid sample damage. This method has been demonstrated on a variety of samples to provide spectroscopic imaging with a spatial resolution as high as 6 nm, as well as complimentary nano-mechanical information.[20,22]

In this communication, we show that PFIR microscopy is a competitive imaging method for studying 2D polaritonic materials. PhPs of hexagonal boron nitride (*h*-BN) were revealed, and their dispersion relations were extracted, similar to studying *h*-BN by using the imaging capability of s-SNOM.[16,23] To increase the signal for thin 2D materials, we developed PFIR microscopy with multiple-pulse excitation.

Peak force infrared microscopy consists of an atomic force microscope (MultiMode, Bruker) with PeakForce Tapping mode and an infrared laser source with customized beam delivery. **Figure 1**a schematically illustrates the PFIR microscope. The frequency-tunable infrared beam from a quantum cascade laser (QCL, MIRcat, Daylight Photonics Solutions) was guided and focused on the tip-sample region of the AFM. The emission of the nanosecond duration QCL pulses was temporally synchronized with the peak force tapping cycle at the moment when the tip and sample are in momentary contact. The repetition rate of the QCL is set to exactly one half of the peak force tapping frequency so that the tip-sample region is illuminated at every other peak force tapping cycle. Detailed experimental parameters are included in Note S1 in the Supporting Information. The dynamic cantilever deflection traces with and without laser illumination were recorded and subtracted to obtain the photothermal expansion response. Figure 1b displays the cantilever deflection traces without (blue trace) and with (red trace) pulsed laser illumination. In this example, the single laser pulse occurs at approximately 80 µs (black trace). The trace without laser is subsequently subtracted from the trace with laser to obtain the pure laser-induced mechanical response (Figure 1c), which is named as PFIR trace. The total amplitude of the laser-induced oscillation of the cantilever is used as the PFIR signal and is derived from the Fourier transform of the PFIR trace (Figure 1d) where we integrate around the laser-induced cantilever oscillation (gray shaded area in Figure 1d). During the measurement, the contact resonance oscillations are excited because the tip end of the cantilever is anchored on the sample. The rapid photothermal expansion excites a wide range of oscillation modes including the higher order mode or contact resonance mode, often more than one peaks are observed as in Figure 1d. In the imaging mode, the PFIR signal is registered while the AFM tip is scanned over the sample. In the spectroscopy mode, the AFM tip is placed at a specific location while the frequency of the laser source is swept across the tunable bandwidth. Note that the photothermal expansion results from relaxations of vibrational modes, such as phonons or phonon polaritons, and the time scale is on the order of picoseconds. As a result, the photothermal expansion behaves like an impulsive excitation and is capable of exciting higher-order resonant modes of the cantilever. The speed of thermal expansion is on the order of 10 to 100 ns,[24] determined by the mechanical properties of the

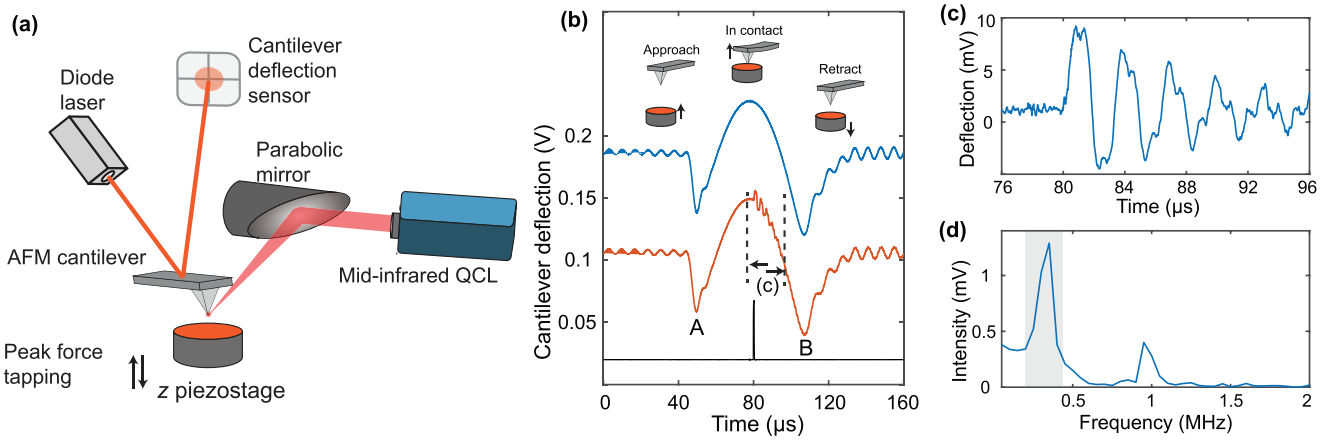

Figure 1. a) Schematic illustration of PFIR microscopy. b) Dynamic cantilever deflection traces in peak force tapping without laser pulse illumination (blue) and with laser pulse illumination (red). The timing of the laser pulse arrival is shown by the black curve. The area between "A" and "B" marks the time when the tip and sample are in contact. c) A PFIR trace is obtained by subtracting the blue curve from the red curve in panel (b). The PFIR trace within the window marked by two dashed lines in panel (b) is shown, which corresponds to the time span 76–96 µs in the peak force tapping cycle. d) Fourier transform of the PFIR trace in panel (c). The integral of laser-induced cantilever oscillations, marked by the gray box, is used as the PFIR signal.

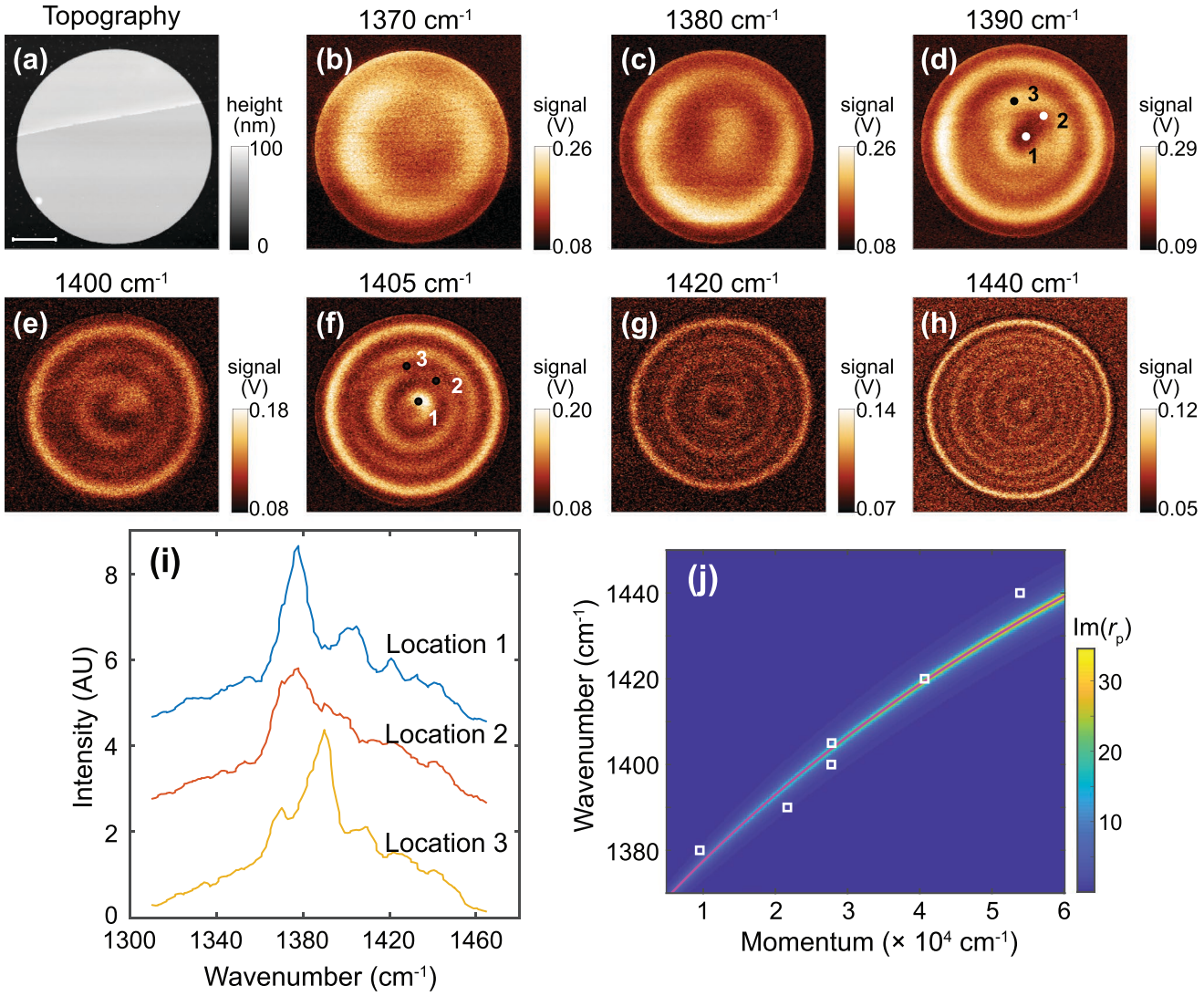

Figure 2. a) Topography of a *h*-^{11}BN disk of 9 µm diameter and 40 nm thickness on SiO_2. The scale bar is 2 µm. b–h) PFIR images of the BN disk at infrared frequencies of 1370–1440 cm^{-1}. The fringes are denser as the laser wavenumbers increase, which is characteristic of the phonon polaritons in *h*-^{11}BN. i) Three PFIR spectra taken from the locations marked in panels (d) and (f). The positions of resonance peaks shift at these locations, which match the observation of different signal intensity of the three locations at different infrared frequencies. j) Extracted dispersion relation of the phonon polaritons on the *h*-^{11}BN microdisk (squares) together with the calculated dispersion relation (red curve) and the false colormap of the imaginary part of the reflectance of *h*-^{11}BN.

sample. Details of the implementation of peak force infrared microscopy are described in the literature.[20]

To demonstrate the method, PFIR images of a 9 µm diameter *h*-^{11}BN microdisk were collected. **Figure 2**a presents the topography of the *h*-^{11}BN microdisk. PFIR images were collected at several infrared frequencies and characteristic wave-like fringes were revealed. Figure 2b–h shows the gradual change of fringe patterns: as the frequency of the light source increases, fringe patterns become denser. The PFIR spectra at three different locations (Figure 2i) were acquired by placing the AFM tip under the peak force tapping feedback and sweeping the frequency of the infrared laser. Three acquiring locations are marked in Figure 2d,f. One can observe variations of spectra at different locations of the microdisk. These variations of PFIR spectra reveal that the infrared absorption of collective tip and sample depends on the position of the tip, due to the propagation and reflection of PhP waves. The phonon polariton modes in the BN microdisk are hyperbolic, where the hybrid electromagnetic field/phonon oscillations extend to both in-plane and out-of-plane direction. In our measurement, the tip touches the sample surface in the perpendicular direction, and the vertically-induced dipole of the tip couples to the out-of-plane component of the hyperbolic phonon polaritons, leading to excitations. Also, when the tip is in contact with the sample, the electromagnetic field is squeezed at the side of the tip, which corresponds to a confined field not strictly perpendicular to the BN surface. Therefore, the in-plane component of phonon polaritons can be coupled as well.

From the spatial patterns in Figure 2c–h, we extracted the energy (ω) and momentum (q_p) dispersion relation of phonon polaritons of this BN microdisk by extracting the spatial frequencies and correlating them with infrared excitation

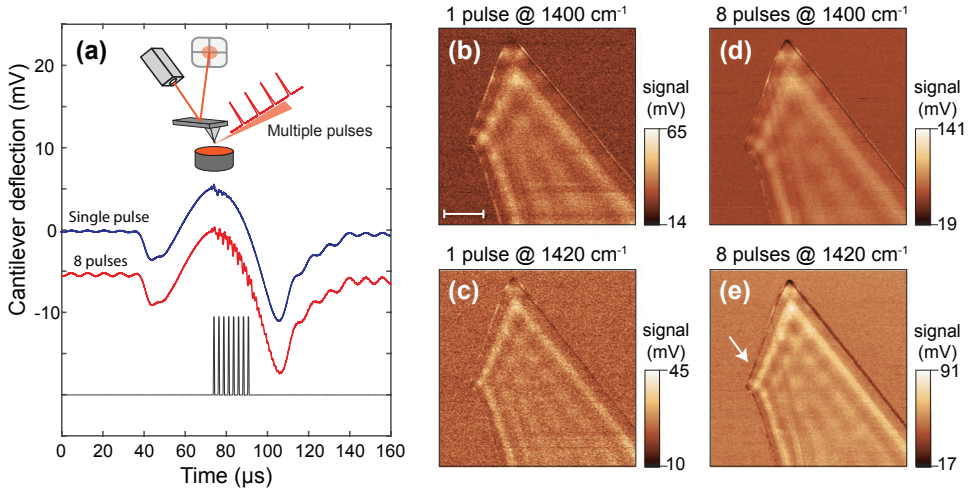

Figure 3. a) Cantilever deflection traces in peak force tapping with one laser pulse (blue), and with eight laser pulses (red). The time of the train of laser pulses is shown as the black curve. The inset shows the scheme of multiple pulse excitation of PFIR. The Q factor of the induced contact resonance in the single-pulse regime is 6.9. b,c) One-pulse PFIR images of an *h*-BN flake at 1400 and 1420 cm^{-1}, respectively. The scale bar is 500 nm. d,e) PFIR images of the *h*-BN flake with excitation of eight infrared pulses and the infrared frequencies are 1400 and 1420 cm^{-1} respectively.

frequencies. Figure 2j displays the measured dispersion relation. As the excitation energy increases, the momentum of launched phonon polaritons correspondingly increases. The calculated plot of the dispersion relation and the false colormap of the imaginary part of the reflectance r_p are included as guidelines in Figure 2j, and was generated with methods described in the literature.[2,25] The details of the calculation are included in Note S2 in the Supporting Information.

One limitation of photothermal AFM microscopy for studying 2D materials is the relatively limited photothermal expansion magnitude due to the small thickness and thermal expansion coefficient of samples. To overcome this limitation, we introduce multiple-pulse excitations into PFIR microscopy. The implementation is conceptually similar to the improvement of the resonantly enhanced infrared nano-spectroscopy (REINS) over conventional PTIR technique in the contact mode.[14] In the new configuration, the QCL laser is triggered to emit a train of laser pulses instead of emitting a single pulse during a peak force tapping cycle. The increased number of photothermal excitation events enhances the PFIR signal. The temporal spacing between the pulses is set equal to the cantilever oscillation period, so that the laser-induced oscillations can coherently add together in phase, considerably amplifying the PFIR signal if the cantilever has a high-quality factor (Q factor). **Figure 3**a illustrates photothermal induced cantilever deflection traces of single-pulse excitation and multipulse excitation. Multiple pulses introduce more photothermal expansion events to excite the cantilever oscillations than a single pulse, increasing the detectable mechanical signal.

The multipulse PFIR microscopy is suitable for the investigation of PhPs in 2D materials with less geometrical confinement and more intrinsic damping. This is demonstrated in Figure 3b–e, which shows PFIR images of a regular, nonisotopically-pure hexagonal BN (*h*-BN) flake. Regular *h*-BN contains both ^{10}B and ^{11}B isotopes, which broaden the phonon mode with more dissipation for phonon polaritons than the isotopically-pure counterpart.[25] The PhPs of the *h*-BN flake were mapped at 1400 and 1420 cm^{-1} with the multipulse PFIR excitation (Figure 3d,e). For comparison, single-pulse PFIR microscopy was used in the same area at the same frequencies (Figure 3b,c). PFIR signals are considerably stronger, and the signal-to-noise ratio is increased from 13 ± 1.2 to 37 ± 1.5, as estimated from the ratio between maximal signal intensity in the PFIR images to the r.m.s. noise from the Si substrate. This signal-to-noise improvement by a factor of 2.8 is consistent with the 2.8^2 (≈8)-fold signal increase from eight times more laser pulses, with a low Q factor cantilever. Subtle features were revealed, such as interference fringes at the edge (marked by a white arrow in Figure 3e). Thus, the imaging capabilities of multipulse PFIR microscopy on the 2D polaritonic material of *h*-BN were demonstrated. We expect the utilization of cantilevers with higher Q factor of contact resonance to further improve the signal quality of the method.

Interestingly, the spatial pattern of polaritonic fringes from PFIR appears to be similar to the reference measurement by s-SNOM (Figure S1, Supporting Information). However, the signal generation mechanism of PFIR microscopy is different from that of s-SNOM. In s-SNOM, as the tip is scanned over the sample, the scattered light is optically detected. The fringes in s-SNOM signal of polaritonic materials come from interference of the tip-launched polariton wave and its reflections from the edges. In contrast, the PFIR signal is not from the optical detection; instead, it registers local photothermal expansion signals. In PFIR, metallic tip in contact with the surface launches polaritonic waves, which propagate and are reflected from the edges. When the reflected wave constructively interferes with the source wave, polaritonic waves are generated stronger than that from the destructive condition. Stronger polaritonic waves lead to more energy absorption from the incident infrared field, resulting in more energy dissipation after the polaritons decay, which causes the photothermal expansion. Therefore, the spatial distribution of photothermal PFIR signals of *h*-BN shares similar spatial patterns as the s-SNOM signal.

In summary, we demonstrated the feasibility of using peak force infrared microscopy to detect and map phonon polaritons in the 2D material of *h*-BN. The photothermal expansion from the sample absorption due to the polaritonic resonance exhibits interference fringe patterns that can be used to reveal the dispersion relation of the polaritons by correlating spatial frequencies and infrared excitation energy. To overcome the intrinsic weak photothermal expansions from 2D inorganic materials, multipulse peak force infrared microscopy was developed to enhance the signal and improve the imaging quality. As an affordable and simple alternative to the scattering-type near-field microscopy, photothermal peak force infrared microscopy will assist future discoveries and investigations of PhPs in 2D materials.

Experimental Section

Sample Preparation: Isotopically pure *h*-^{11}BN crystalline flakes were grown from a molten metal nickel–chromium solution using boron-11 as the boron source.[26] The *h*-^{11}BN flake was exfoliated using tape and transferred on a silicon wafer substrate with 285 nm of thermal oxide. E-beam lithography and reactive ion etching were used on the *h*-^{11}BN to create a microdisk for the PFIR measurement. Regular *h*-BN flakes were obtained through exfoliation and used for multipulse PFIR measurement.

Supporting Information

Supporting Information is available from the Wiley Online Library or from the author.

Acknowledgements

The authors cordially thank for the fruitful discussions and the help from Dr. Antonio Ambrosio and Dr. Michele Tamagnone on the polaritonic behaviors of the *h*-^{11}BN microdisk. The authors would like to also thank Dr. William L. Wilson of Center for Nanoscale Systems of Harvard University for the fabrication of the BN microdisk. L.W., H.W., and X.G.X. would like to thank the support from National Science Foundation CHE 1847765. X.G.X. would like to thank the Arnold and Mabel Beckman Foundation for Beckman Young Investigator Award. J.L. and J.H.E. thank the support from National Science Foundation, award number CMMI 1538127.

Conflict of Interest

Martin Wagner is an employee of Bruker, which provides commercially available AFMs with peak force tapping capability. Other authors declare no conflict of interest.

Keywords

hexagonal boron nitride, nano-IR spectroscopy, peak force infrared microscopy, phonon polaritons, s-SNOM

Received: June 28, 2019
Revised: October 7, 2019
Published online:

[1] D. N. Basov, M. M. Fogler, F. J. García de Abajo, *Science* **2016**, *354*, aag1992.
[2] S. Dai, Z. Fei, Q. Ma, A. S. Rodin, M. Wagner, A. S. McLeod, M. K. Liu, W. Gannett, W. Regan, K. Watanabe, T. Taniguchi, M. Thiemens, G. Dominguez, A. H. C. Neto, A. Zettl, F. Keilmann, P. Jarillo-Herrero, M. M. Fogler, D. N. Basov, *Science* **2014**, *343*, 1125.
[3] Z. Fei, G. O. Andreev, W. Bao, L. M. Zhang, A. S. McLeod, C. Wang, M. K. Stewart, Z. Zhao, G. Dominguez, M. Thiemens, *Nano Lett.* **2011**, *11*, 4701.
[4] E. Abbe, *Arch. Mikrosk. Anat.* **1873**, *9*, 413.
[5] L. Novotny, S. J. Stranick, *Annu. Rev. Phys. Chem.* **2006**, *57*, 303.
[6] Z. Fei, A. S. Rodin, G. O. Andreev, W. Bao, A. S. McLeod, M. Wagner, L. M. Zhang, Z. Zhao, M. Thiemens, G. Dominguez, M. M. Fogler, A. H. C. Neto, C. N. Lau, F. Keilmann, D. N. Basov, *Nature* **2012**, *487*, 82.
[7] a) J. Chen, M. Badioli, P. Alonso-González, S. Thongrattanasiri, F. Huth, J. Osmond, M. Spasenović, A. Centeno, A. Pesquera, P. Godignon, A. Zurutuza Elorza, N. Camara, F. J. G. de Abajo, R. Hillenbrand, F. H. L. Koppens, *Nature* **2012**, *487*, 77; b) A. J. Huber, D. Kazantsev, F. Keilmann, J. Wittborn, R. Hillenbrand, *Adv. Mater.* **2007**, *19*, 2209; c) S. Dai, J. Zhang, Q. Ma, S. Kittiwatanakul, A. McLeod, X. Chen, S. G. Corder, K. Watanabe, T. Taniguchi, J. Lu, Q. Dai, P. Jarillo-Herrero, M. Liu, D. N. Basov, *Adv. Mater.* **2019**, *31*, 1900251.
[8] F. Keilmann, R. Hillenbrand, *Philos. Trans. R. Soc., A* **2004**, *362*, 787.
[9] X. Chen, D. Hu, R. Mescall, G. You, D. Basov, Q. Dai, M. Liu, *Adv. Mater.* **2019**, *31*, 1804774.
[10] F. Hu, Y. Luan, M. E. Scott, J. Yan, D. G. Mandrus, X. Xu, Z. Fei, *Nat. Photonics* **2017**, *11*, 356.
[11] Z. Zheng, J. Chen, Y. Wang, X. Wang, X. Chen, P. Liu, J. Xu, W. Xie, H. Chen, S. Deng, N. Xu, *Adv. Mater.* **2018**, *30*, 1705318.
[12] A. Centrone, *Annu. Rev. Anal. Chem.* **2015**, *8*, 101.
[13] a) A. Dazzi, C. B. Prater, Q. Hu, D. B. Chase, J. F. Rabolt, C. Marcott, *Appl. Spectrosc.* **2012**, *66*, 1365; b) A. M. Katzenmeyer, V. Aksyuk, A. Centrone, *Anal. Chem.* **2013**, *85*, 1972.
[14] F. Lu, M. Jin, M. A. Belkin, *Nat. Photonics* **2014**, *8*, 307.
[15] a) A. Ambrosio, L. A. Jauregui, S. Dai, K. Chaudhary, M. Tamagnone, M. M. Fogler, D. N. Basov, F. Capasso, P. Kim, W. L. Wilson, *ACS Nano* **2017**, *11*, 8741; b) C. Ciano, V. Giliberti, M. Ortolani, L. Baldassarre, *Appl. Phys. Lett.* **2018**, *112*, 153101.
[16] L. V. Brown, M. Davanco, Z. Sun, A. Kretinin, Y. Chen, J. R. Matson, I. Vurgaftman, N. Sharac, A. J. Giles, M. M. Fogler, T. Taniguchi, K. Watanabe, K. S. Novoselov, S. A. Maier, A. Centrone, J. D. Caldwell, *Nano Lett.* **2018**, *18*, 1628.
[17] D. Nowak, W. Morrison, H. K. Wickramasinghe, J. Jahng, E. Potma, L. Wan, R. Ruiz, T. R. Albrecht, K. Schmidt, J. Frommer, D. P. Sanders, S. Park, *Sci. Adv.* **2016**, *2*, e1501571.
[18] a) K. Wieland, G. Ramer, V. U. Weiss, G. Allmaier, B. Lendl, A. Centrone, *Nano Res.* **2019**, *12*, 197; b) J. Mathurin, E. Pancani, A. Deniset-Besseau, K. Kjoller, C. B. Prater, R. Gref, A. Dazzi, *Analyst* **2018**, *143*, 5940.
[19] a) J. Jahng, E. O. Potma, E. S. Lee, *Anal. Chem.* **2018**, *90*, 11054; b) J. Yamanishi, Y. Naitoh, Y. J. Li, Y. Sugawara, *Appl. Phys. Lett.* **2017**, *110*, 123102.
[20] L. Wang, H. Wang, M. Wagner, Y. Yan, D. S. Jakob, X. G. Xu, *Sci. Adv.* **2017**, *3*, e1700255.
[21] C. Su, *Microsc. Microanal.* **2010**, *16*, 364.
[22] D. S. Jakob, L. Wang, H. Wang, X. G. Xu, *Anal. Chem.* **2019**, *91*, 8883.
[23] a) F. J. Alfaro-Mozaz, P. Alonso-González, S. Vélez, I. Dolado, M. Autore, S. Mastel, F. Casanova, L. E. Hueso, P. Li, A. Y. Nikitin, R. Hillenbrand, *Nat. Commun.* **2017**, *8*, 15624; b) S. Dai, J. Quan, G. Hu, C.-W. Qiu, T. H. Tao, X. Li, A. Alù, *Nano Lett.* **2019**, *19*, 1009;

c) S. Dai, Q. Ma, Y. Yang, J. Rosenfeld, M. D. Goldflam, A. McLeod, Z. Sun, T. I. Andersen, Z. Fei, M. Liu, Y. Shao, K. Watanabe, T. Taniguchi, M. Thiemens, F. Keilmann, P. Jarillo-Herrero, M. M. Fogler, D. N. Basov, *Nano Lett.* **2017**, *17*, 5285; d) S. Dai, M. Tymchenko, Y. Yang, Q. Ma, M. Pita-Vidal, K. Watanabe, T. Taniguchi, P. Jarillo-Herrero, M. M. Fogler, A. Alù, D. N. Basov, *Adv. Mater.* **2018**, *30*, 1706358.

[24] L. V. Wang, J. Yao, *Nat. Methods* **2016**, *13*, 627.

[25] A. J. Giles, S. Dai, I. Vurgaftman, T. Hoffman, S. Liu, L. Lindsay, C. T. Ellis, N. Assefa, I. Chatzakis, T. L. Reinecke, J. G. Tischler, M. M. Fogler, J. H. Edgar, D. N. Basov, J. D. Caldwell, *Nat. Mater.* **2018**, *17*, 134.

[26] S. Liu, R. He, L. Xue, J. Li, B. Liu, J. H. Edgar, *Chem. Mater.* **2018**, *30*, 6222.